frontiers | Frontiers in Earth Science

ORIGINAL RESEARCH
published: 19 April 2022
doi: 10.3389/feart.2022.879297

Inclusion Characteristics of the Fracture-Cave Calcite of Ordovician Yingshan Formation and Its Indication to the Formation of Paleokarst Reservoir in the Northern Slope of Tarim Basin Center Area, China

Yong Dan[1,2], *Junjie Ba*[1,2]*, *Bin Liang*[1,2], *Qingyu Zhang*[1,2], *Jingrui Li*[1,2] *and Guoquan Nie*[1,2]

[1]*Institute of Karst Geology, Chinese Academy of Geological Sciences/Karst Dynamics Laboratory, Guilin, China,* [2]*International Research Center on Karst Under the Auspices of UNESCO, Guilin, China*

OPEN ACCESS

Edited by:
Hao Zou,
Chengdu University of Technology, China

Reviewed by:
Guoqing Xiong,
Chengdu Geological Survey Center, China
Bo Peng,
Chinese Academy of Geological Sciences (CAGS), China

***Correspondence:**
Junjie Ba
bajunjie@karst.ac.cn

Specialty section:
This article was submitted to Economic Geology, a section of the journal Frontiers in Earth Science

Received: *19 February 2022*
Accepted: *07 March 2022*
Published: *19 April 2022*

Citation:
Dan Y, Ba J, Liang B, Zhang Q, Li J and Nie G (2022) Inclusion Characteristics of the Fracture-Cave Calcite of Ordovician Yingshan Formation and Its Indication to the Formation of Paleokarst Reservoir in the Northern Slope of Tarim Basin Center Area, China. Front. Earth Sci. 10:879297. doi: 10.3389/feart.2022.879297

A karst fracture-cavity was developed in the Ordovician Yingshan Formation in the northern slope of the Tarim Basin center area (Tazhong area); however, the area experienced multistage karst and diagenesis in the later period, and the reservoir was heavily reformed, characterized by complex distribution. Based on the testing of the inclusions in the karst fractures and fracture-cave calcite, this study summarizes the physical and chemical characteristics of the inclusions in the northern slope of Tazhong. The major inclusions were liquid and gas–liquid phases, while the minor ones were hydrocarbon phases. Based on the salinity–homogenization temperature diagram, the gas–liquid inclusions could be divided into seven types: low-temperature low-salinity inclusions (the lowest salinity was 0.88%, which is lower than that of present sea water; the lowest temperature of the inclusions was 49°C); low-temperature high-salinity inclusions; medium-temperature low-salinity inclusions; medium-temperature medium-salinity inclusions; medium-temperature high-salinity inclusions; high-temperature medium-salinity inclusions; and high-temperature high-salinity inclusions. The development of inclusions was characterized by high temperature and high salinity or low temperature and low salinity. In addition, the low-temperature and low-salinity inclusions near the unconformity surface were well-developed. The high-temperature and higher-salinity inclusions far from the unconformity surface were also well-developed. A burial history analysis showed three stages of karstification or filling in the area: exposed karstification in the Middle Caledonian, shallow burial filling in the Middle Hercynian, and burial filling in the Late Hercynian. By determining the inclusions in calcite associated with mud in the karst caves and combined with previous studies, the Middle Caledonian was found to be the period associated with the eogenetic karstification of meteoric water and seawater. This is the key factor in the formation of karst reservoirs in the Tazhong area. The large-scale calcite growth in the Middle Hercynian and Late Hercynian burial periods led to further filling of the early karst reservoir, reduced reservoir space, and enhanced reservoir heterogeneity.

Keywords: inclusion, fracture-cavity reservoir, Yingshan formation, buried karst, homogenization temperature, burial history, eogenetic karstification

1 INTRODUCTION

Since the 1990s, the Ordovician carbonate fracture-cavity oil and gas field located in the Tarim Basin has been continuously explored and developed. It has been the most important oil and gas exploration field in China and continues to have significant exploration potential (Yang et al., 2011). Previous studies have shown that the long-term exposure of meteoric water karst in the Caledonian–Hercynian period led to development of karst caves in the Ordovician in the northern Tarim Basin (Yan et al., 2002; Yan et al., 2005; He et al., 2007; Dan et al., 2012). Since 2006, several karst hole–type oil and gas reservoirs have been discovered in the Middle and Lower Ordovician Yingshan Formations in the Tazhong area (Yang et al., 2011). Unlike the karst in the northern region (which has an exposure time of more than 200 Ma) (Chen et al., 2004; Zhu et al., 2009; Zhao et al., 2013), the top of the Yingshan Formation in Tazhong has few lacunas, and the exposure time is generally short (approximately in the range of 7–11 Ma). The karst holes in the Yingshan Formation are small but many, and they contain vast inclusions (Yang et al., 2011; Ni et al., 2013; Pang et al., 2013; Dan et al., 2015). Regarding the origin of these types of karst holes, previous studies have suggested that they are similar to those formed in the north of the Tarim Basin in the early stage—the development of the holes was mainly controlled by the meteoric water in the Caledonian period and then by the buried karst in the later stage (Yang et al., 2011; Ni et al., 2013; Pang et al., 2013). In recent years, scholars have conducted in-depth studies on the characteristics of fracture-cavity karst morphology, distribution law, and inclusion geochemistry (carbon and oxygen isotopes; major, trace, and rare earth elements); eogenetic karstification was proven to be the origin of the karst in this area. Larger caves were more likely to develop in mixed-water karst zones controlled by sea level (Dan et al., 2015; Chen et al., 2016; Zhang et al., 2016; Dan et al., 2018; Dan et al., 2019; Dan et al., 2021). Nonetheless, the above mentioned studies did not provide direct evidence of karst fluid salinity, temperature, etc.

Fluid inclusions are diagenetic fluids trapped in crystal defects during mineral crystallization, which record the information of diagenetic fluids. They are widely used in the study of petroleum geology as a technical tool, such as the morphology, composition, and homogenization temperature characteristics of the inclusions in fractures and caves. They directly reflect the fluid characteristics and environmental conditions at the time of their formation (Lu, 1990). The dissolution and inclusion growth in carbonate rocks occurs simultaneously. The fluid inclusions developed during the growth of calcite from fracture-caves can reflect the information of karst fluids to some extent and are also a good indicator of the paleokarst environment and stages (Lu, 1990; Liu, 1991; Chen et al., 2003; Chen et al., 2004; Xia and Tang, 2004; Xia et al., 2006; Liu et al., 2007; Cai et al., 2009; Wu et al., 2010; Dan et al., 2015). Analyzing the inclusions has become an important tool in the study of paleokarstification.

Given the lack of clear data on the karst stages and karst fluid environment of the Yingshan Formation in the Tazhong area, the inclusions in calcite were sampled from the fracture-caves in drilling cores and then tested to obtain relevant parameters. The results provide relevant evidence to judge the nature of the paleokarst fluid and karst environment formed in the fracture-cave of the Yingshan Formation. They can promote the study of the genetic mechanism of fracture-cavity reservoirs in the Yingshan Formation in the northern slope of the Tazhong area and can provide a basis for establishing paleokarst reservoir prediction models and guiding oil and gas exploration in the Tazhong area.

2 GEOLOGICAL SETTING

The Tazhong Uplift is oriented NW–SE, with the Bachu fault uplifted to the west, lower Tadong bulging to the east, Manjiaer Sag located to the north, and Tongguzabasi Depression to the south (Shu et al., 2008) (**Figure 1A**). It is divided into three subtectonic belts from north to south: northern slope, central fault horst, and southern slope (Lan et al., 2014). The study area is located in the northern slope between the central-faulted horst belt and Tazhong No. I fault zone (**Figure 1A**). During the Early Ordovician–Middle Ordovician period, the Tazhong area was in a relatively stable tectonic setting, and the Yingshan Formation comprised a set of calcarenite and micrite of carbonate platform facies (Pang et al., 2013).

The northern slope of Tazhong has experienced four main tectonic movements (Quan, 2020): Cambrian Early Ordovician extensional environment and development of extensional faults; under the influence of Caledonian tectonic movement in the middle and late Ordovician, the study area was subjected to NE–SW compression; a large-scaled thrust system of trending NWW, such as the Tazhong No. I fault zone, was formed due to the influence of the tectonic movement of Caledonian I. In addition, Middle–Lower Ordovician carbonate rocks were entirely uplifted as a result of regional compression. The carbonate platform was exposed and underwent intense erosion and karstification, leading to formation of the unconformity surface of the Yingshan Formation (**Figure 1**) (Yu et al., 2011; Chen et al., 2016). In the high part of the uplift, the Middle Ordovician Yijianfang Formation and Upper Ordovician Tumuxiuke Formation were missing due to severe denudation. The Middle–Lower Ordovician Yingshan Formation also underwent denudation. From Silurian to Devonian, strike slip faults were developed under continuous compression from northeast to southwest. In the Permian, due to subduction, a large number of volcanic activities developed tensile fractures. In the Cambrian Early Ordovician tectonic activity stage, the Ordovician Yingshan Formation was not deposited and had no direct impact on the formation of the target reservoir (Quan, 2020).

Currently, the Ordovician formation can be divided (from top to bottom) into the following formations: Sangtamu, Lianglitage, Yingshan, and Penglaiba (**Figures 1B,C**). The depositional break between the Yingshan and Lianglitage Formations lasted for approximately 12–15 Ma (Yu et al., 2011; Chen et al., 2016). The exposed karstification of the Yingshan Formation lasted for 7–11 Ma. The Yingshan Formation in the northern slope of

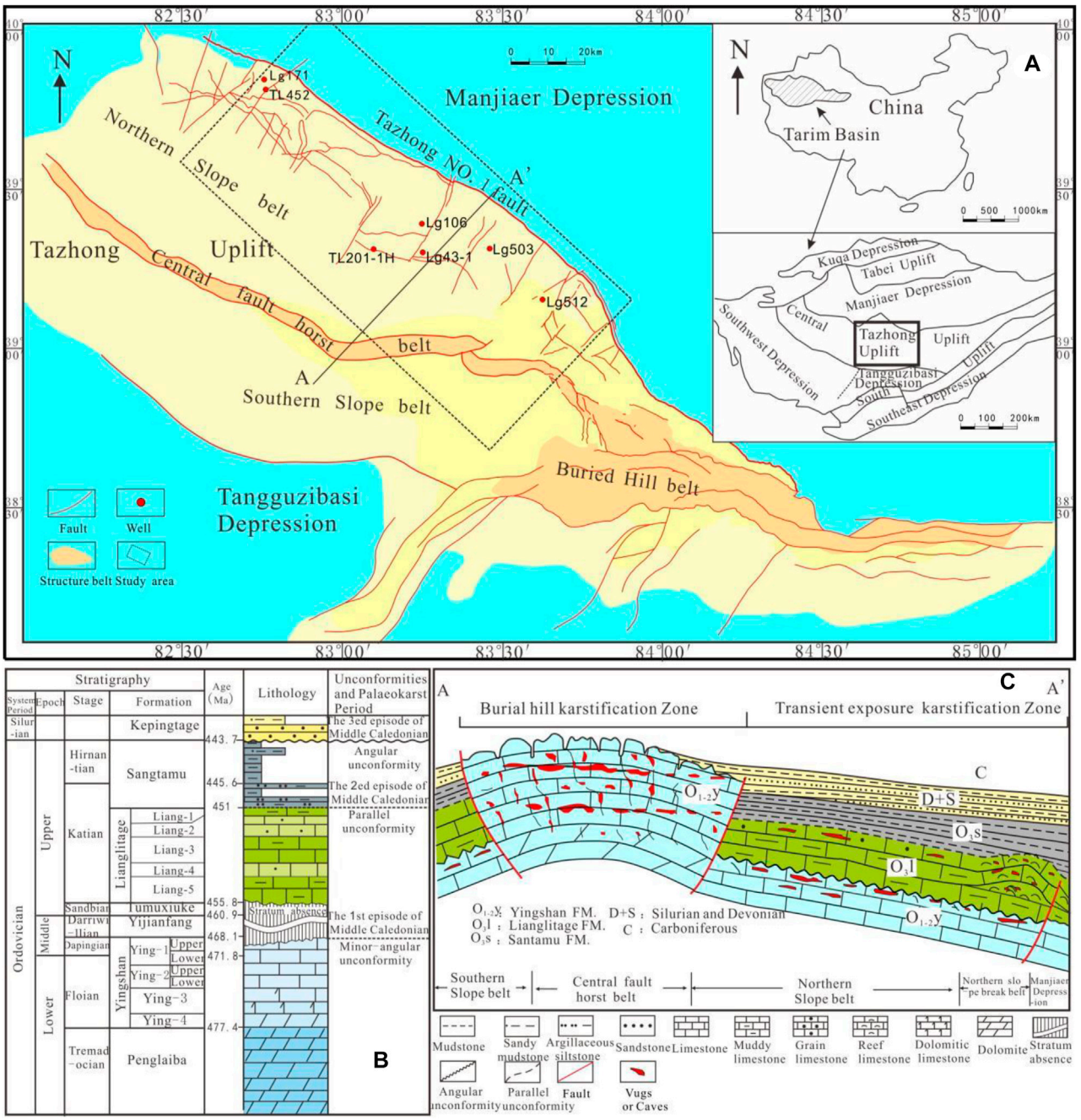

FIGURE 1 | Sketch of the structural features in the Tazhong area. **(A)** Tectonic division of the Tazhong Uplift and location of the study area; **(B)** Generalized stratigraphy and associated reservoir intervals (northern slope belt) of the Yingshan Formation in the study area. **(C)** Karstification division of the Tazhong Uplift and location of the northern slope belt.

Tazhong can be divided into four members (**Figure 1B**) based on the well-logging electrical properties (**Figure 1B**). Ying-1 and Ying-2 members comprise pure limestone with a thickness of approximately 300 m, whereas Ying-3 and Ying-4 members comprise dolomitic limestone and dolomite.

The unconformity exposed strata comprise limestone from the Ying-1 and Ying-2 members, which are noneffective reservoirs having low porosity and low permeability, with an average porosity of 0.91% and a permeability of 3.76×10^{-3} μm^2 (Yang et al., 2011). The present reservoir is mainly the secondary fracture-cave reservoir formed under the impact of the karstification and tectonic movement at the late stage, and it is an important oil and gas reservoir in the Tarim Basin. Its effective reservoir space consists of mainly karst holes, caves, and fractures

(Feng et al., 2014). These fractures and caves are distributed within 300 m below the unconformity surface and often filled with calcite, clay, and organic matter (Dan et al., 2018). The large karst caves are considered the main reservoir space and are mostly filled with clay, limestone breccias, and calcite (Dan et al., 2018). A total of 107 karst caves (with a height of more than 0.3 m) have been discovered in 90 wells in the study area, among which 62 karst caves are filled, accounting for 57.94% (Dan et al., 2018). The currently unfilled reservoirs are mainly developed in the lower part of the filled section (Dan et al., 2018). To understand the formation mechanism of most fracture-cavities of the Yingshan Formation, the formation and filling environment of the karst caves should be determined by sampling and analyzing the inclusions in the caves.

3 SAMPLING AND TESTING

3.1 Sample Collection of Calcite From the Fracture Cave at Different Stages

The samples were mainly taken from the carbonate strata of the Ordovician Yingshan Formation on the northern slope of the Tazhong area. In addition to the calcite taken from the karst cave, calcite was also taken from the cracks. As for the fracture stages, the fracture stages in the Tazhong area have been studied by conducting acoustic emission experiments. Three stages of fractures have been considered to mainly develop in the study area: calcite-filled structural fractures formed in the Silurian Devonian and Late Hercynian; it was formed in the unfilled structural fracture of the Himalayan period (Xu et al., 2012). On this basis, the geometric shape and cutting relationship of the fractures in the rock core were determined. The results showed the development of multistage fractures in the study area, and the sequence of fracture development was as follows: 1) Horizontal suture (mainly filled with organic matter and black argillaceous matter); 2) High-angle suture; 3) Dissolution fractures (holes) are formed by dissolution expansion and filled with grayish–green mud with different occurrences; 4) High-angle shear joints filled with white calcite or translucent, with local joints also having the characteristics of solution expansion; 5) White calcite-filled horizontal structural fine joints; 6) Horizontal opening seam; and 7) High-angle opening seam. Quan (2020) considered the formation of stages 1 horizontal suture and 2 a high-angle suture between the Middle and Late Ordovician and Silurian. Stage 3 is the dissolution fracture formed during the exposure period of the Middle–Late Ordovician by the dissolution expansion along the early suture and the fractures in the same period during the exposure period; it is filled with terrigenous argillaceous material. The white or translucent calcite-filled shear fractures or solution fractures were formed in the Middle–Late Ordovician and Silurian Devonian. 5) The origin of the white-calcite-filled horizontal structural fine fracture is unclear; it was formed after the formation of the Silurian Devonian shear fracture. The open joints of the stages 6 and 7 were formed in the Himalayan tectonic stage. Megacryst calcite precipitates (>2 cm) were found in seven of the 40 rock cores, with mainly argillaceous inclusions in the fractures and caves. The collected samples are mainly from the 3) and 4) stages, and the types include coarse-grained calcite filled in the 4) stage high-angle solution fracture and coarse-grained calcite filled in the 4) stage high-angle structural fracture. In addition, to study the karst fluid properties of the karst cave filled with mud during the exposure period in the northern slope of the Tazhong area, a microscope and cathodoluminescence instrument are specially used to select the calcite filled with mud from the 3) stage fracture and cave. The interlayer joints were filled with calcite in calcareous mudstone (**Figure 2**). There were eight samples mainly located 0–210 m below the unconformity surface at the top of the Yingshan Formation, obtained from six wells (**Table 1**).

3.2 Test Method

Petrographic and cathodoluminescence (CL) analyses were conducted on five thin sections of the samples. A cold cathode luminescence microscope was used with a beam voltage of 17 kV and a beam current of 500 μA on all the samples. The CL8200 MK5 cathode luminescence analyzer (CITL, United Kingdom, in conjunction with a Leica polarizing microscope) was used for the cathode luminescence analysis. The inclusion slices from the samples were grinded and then tested using the THMSG600 heating/freezing stage (Linkam Company, United Kingdom). The inclusion test was conducted in the Analysis and Testing Research Center of Beijing Institute of Geology, China Nuclear Industry Geological Bureau.

4 RESULTS

4.1 Physical Characteristics of Inclusions

Lu (1990) considered that the inclusions contained in calcite are mainly primary inclusions; the test results showed that they were primary inclusions and were not divided into primary and secondary. The inclusions were mainly liquid inclusions at room temperature, including some hydrocarbon inclusions. The liquid inclusions mainly existed in the liquid phase, while a few existed in the gas–liquid phase (**Table 1**). The liquid-phase inclusions were mainly round and oval, colorless, and transparent under the microscope, with a size range of 2–15 μm (some of 50 μm). The liquid-phase inclusions were generally smaller than the gas–liquid inclusions and were distributed in groups or strips along the microfractures in the calcite crystals (**Figure 3A**). The gas–liquid phase inclusions were mainly round, rectangular or polygonal, colorless, and transparent under the microscope, with a size range of 3–20 μm (some had a size of 80 μm). They were distributed in groups, uniformly, or in strips in the calcite (**Figure 3B**). **Table 1** shows that except for sample no. 6, the liquid-phase inclusions in the other samples account for more than 35–40% of the total inclusions. Moreover, all the samples contained more or less hydrocarbon inclusions, indicating the abundance of oil and gas in the northern slope of the Tazhong area.

FIGURE 2 | Calcite development in the fractures and caves of the Yingshan Formation in the northern slope of the Tazhong area. **(A)** Calcite filled in period 4 fractures, LG106, 2 (44/58), 6,074.4 m. **(B)** Calcite filled in high-angle fractures in period 4, LG503, 1 (23/53), 5,942.4 m. **(C)** Calcite filled in period 4) fractures, LG171, 4 (23/74), 6,493 m. **(D)** Calcite filled in period 4 fractures. The opening joints of periods 6 and 7, LG512, 4 (4/70), 5,582.5 m. **(E)** Calcite filled in high-angle fractures, where the suture can be seen in period 1, TL452, 3 (22/43), 6,461 m. **(F)** Calcite filled in period 4 structural fractures, LG512, 4 (49/70), 5,587.6 m. **(G)** Calcite filled in a 40-cm-long cave, which is completely filled with calcareous argillaceous (limestone gravel and grayish–green calcareous clay) fillings; it is the stage 3 of exposed karst formation, TL201-1H, 4 (46/62), 5,460.6–6,461 m. **(H)** Calcite filled in period 3 inter-formational fractures with grayish-green calcareous mudstone, LG512, 3 (36/58), 5,484.3 m. **(I)** Micrograph at the white circle in **(G)**, containing dissolved and dissociated limestone debris particles (Gr), clay (Cl), and calcite (Cal), TL201-1H, 4 (46/62), 5,460.7 m **(J)** cathodoluminescence image of **(I)**, in which the sandy sparite limestone is weak–moderately luminous, with luminous bands at the edges, while calcite is not luminous.

TABLE 1 | Outcomes of calcite samples and physical characteristics of inclusions in the northern slope of the Tazhong area.

No.	Sampling well	Distance[a]	Calcite occurrence	Inclusions				
				Phase state	Proportion (%)	Size (μm)	Shape	Inclusion distribution
1	LG106 2 (44/58)	0	In fracture	Gaseous hydrocarbons	10	3–5	Round, oval	Group/strip distribution along the micro fractures
				Liquid hydrocarbons	15	2–20	Irregular, rectangle	Group/strip distribution along the micro fractures
				Liquid	45	2–20	Round, square	Group, uniform/strip distribution
				Gas–liquid	30	3–25	Round, polygon	Group, uniform/strip distribution
2	LG503 1 (23/53)	3	In high-angle fracture	Gaseous hydrocarbons	10	4–10	Round, oval	Group/strip distribution along the microfractures
				Liquid hydrocarbons	1	4–10	Irregular, rectangle	Line distribution along the microfractures
				Gas–liquid hydrocarbons	4	3–15	Irregular, square	Group/strip distribution along the microfractures
				Liquid	40	2–20	Round, polygon	Group, uniform/strip distribution
				Gas–liquid	45	2–40	Round, polygon	Group, uniform/strip distribution
3	TL201-1H 4 (46/62)	18	In cavity with mud	Gaseous hydrocarbons	10	3–8	Round, oval	Group/strip distribution along the microfractures
				Liquid hydrocarbons	15	2–10	Irregular, rectangle	Group/strip distribution along the microfractures
				Liquid	55	2–10	Round, oval	Group, uniform/strip distribution
				Gas–liquid	20	3–15	Round, polygon	Group, uniform/strip distribution
4	TL452 3 (22/43)	100	In fracture	Gaseous hydrocarbons	8	3–6	Round, oval	Group/strip distribution along the microfractures
				Liquid hydrocarbons	15	2–20	Irregular, rectangle	Group/strip distribution along the microfractures
				Liquid	45	2–20	Round, square	Group, uniform/strip distribution
				Gas–liquid	32	3–15	Round, polygon	Group, uniform/strip distribution
5	LG512 3 (36/58)	104	In interlayer fracture with calcareous Mudstone	Gaseous hydrocarbons	10	4–10	Round, oval	Group/strip distribution along the microfractures
				Liquid hydrocarbons	3	3–10	Irregular, rectangle	Line distribution along the microfractures
				Gas–liquid hydrocarbons	5	2–10	Irregular, square	Group/strip distribution along the microfractures
				Liquid	32	3–50	Round, polygon	Group, uniform/strip distribution
				Gas–liquid	50	2–80	Round, polygon	Group, uniform/strip distribution
6	LG171 4 (23/74)	108	In fracture	Gaseous hydrocarbons	15	2–10	Round, oval	Group, uniform/strip distribution
				Liquid hydrocarbons	20	2–10	Irregular, rectangle	Group, uniform/strip distribution
				Liquid	25	2–20	Round, square	Group, uniform/strip distribution
				Gas–liquid	40	3–20	Round, polygon	Group, uniform/strip distribution
7	LG512 4 (4/70)	207	In fracture	Gaseous hydrocarbons	8	4–15	Round, oval	Group/strip distribution along the microfractures
				Liquid hydrocarbons	12	3–10	Irregular, rectangle	Line distribution along the microfractures
					10	2–10		

(Continued on following page)

TABLE 1 | (*Continued*) Outcomes of calcite samples and physical characteristics of inclusions in the northern slope of the Tazhong area.

No.	Sampling well	Distance[a]	Calcite occurrence	Inclusions				
				Phase state	Proportion (%)	Size (μm)	Shape	Inclusion distribution
				Gas–liquid hydrocarbons			Irregular, square	Group/strip distribution along the microfractures
				Multiphase hydrocarbon	3	2–15	Irregular, square	Group/strip distribution along the microfractures
				Liquid	37	3–40	Round, polygon	Group, uniform/strip distribution
				Gas–liquid	30	2–50	Round, polygon	Group, uniform/strip distribution
8	LG512 4 (49/70)	210	In structural fracture	Gaseous hydrocarbons	15	4–10	Round, oval	Group/strip distribution along the microfractures
				Liquid hydrocarbons	2	3–10	Irregular, rectangle	Line distribution along the microfractures
				Gas–liquid hydrocarbons	8	2–15	Irregular, square	Group/strip distribution along the microfractures
				Liquid	40	3–30	Round, polygon	Group, uniform/strip distribution
				Gas–liquid	40	2–40	Round, polygon	Group, uniform/strip distribution

[a]*Distance to the top of the Yingshan Formation.*

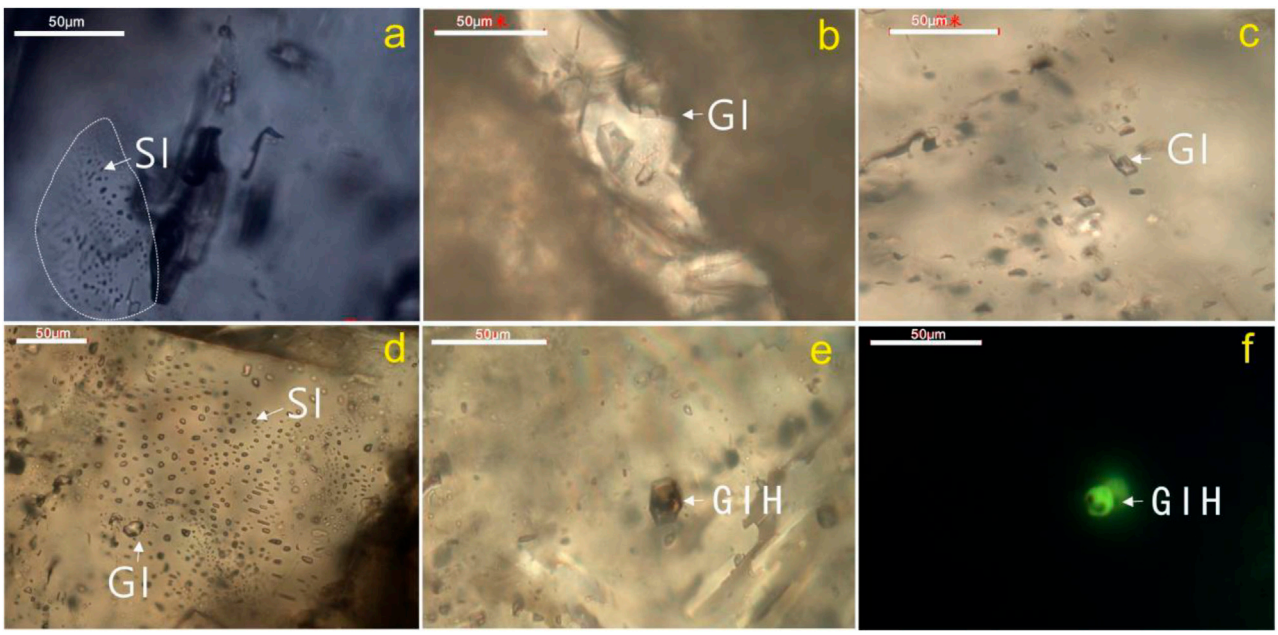

FIGURE 3 | Shapes and distribution characteristics of inclusions. **(A)** Group-distributed liquid inclusions (SI) in calcite of period 3 karst cave, TL201-1H; **(B)** gas–liquid (GI) distributed inclusions in calcite, TL452; **(C)** group-distributed inclusions in calcite of period 4) crack, LG106; **(D)** inclusions distributed along the microfractures of period 4) crack, LG512 **(E,F)** inclusions distributed in the gas–liquid–hydrocarbon (GIH) phase of period 4 cracked calcite, while the liquid hydrocarbon phase is yellow-green under UV fluorescence excitation.

4.2 Chemical Characteristics of Gas–Liquid Phase Inclusions

In this study, 273 gas–liquid phase inclusions were selected from eight samples to measure the freezing point temperature, initial dissolving temperature, and homogenization temperature. The salinity was calculated on the basis of the conversion relationship between the freezing point temperature and NaCl salinity, which was proposed by Bodnar (1992). **Table 2** presents the results.

TABLE 2 | Chemical characteristics of the gas–liquid phase inclusions in Ordovician calcite from the northern slope of the Tazhong area.

No.	Sampling well	Depth (m)	Distance[a] (m)	Calcite formation	Phase	Freezing point T (°C)	Homogenization T (°C)	w (NaCl)%	Initial dissolving T (°C)	Water-salt system
1	LG106 2 (44/58)	6,074.4	0	In fracture	Gas–liquid1	−4.8to−0.8	78–105	1.4–7.59	−23.2to−22.4	NaCl-KCl-H_2O
					Gas–liquid2	−20.1to−18.4	66–90	21.26–22.38	−35.5to−34.4	NaCl-H_2O-$MgCl_2$
2	LG503 1 (23/53)	5,942.4	3	In high-angle fracture, coarse crystals	Gas–liquid	−20 to −19.4	63–111	21.96–22.38	−54.1 to −52.5	$CaCl_2$-NaCl-H_2O
3	TL201-1H 4 (46/62)	5,460.7	18	In cavity with mud	Gas–liquid	−14.1 to −1.5	49–116	2.57–17.87	−23.0 to −22.2	NaCl-KCl-H_2O
4	TL452 3 (22/43)	6,461	100	In fracture	Gas–liquid	−11 to −1.1	79–119	1.91–14.97	−35.0 to −34.4	NaCl-H_2O-$MgCl_2$
5	LG512 3 (36/58)	5,484.3	104	In interlayer fracture with Calcareous Mudstone	Gas–liquid1	−20 to −6.8	78–128	10.24–22.38	−34.8 to −32.2	NaCl-H_2O-$MgCl_2$
6	LG171 4 (23/74)	6,493	108	In fracture	Gas–liquid	−20 to −0.5	56–106	0.88–22.38	−49.0 to −47.5	$CaCl_2$-NaCl-H_2O
7	LG512 4 (4/70)	5,582.5	207	In fracture	Gas–liquid	−20 to −16	68–100	19.53–22.38	−35.3 to −33.8	NaCl-H_2O-$MgCl_2$
8	LG512 4 (49/70)	5,587.6	210	In structural fracture	Gas–liquid1	−20 to −12.4	75–113	16.34–22.38	−35.6 to −34.5	NaCl-H_2O-$MgCl_2$

[a]*Depth to the top of the Yingshan Formation.*

4.2.1 Salinity Characteristics of Gas–Liquid Phase Inclusions

Based on the salinity distribution chart of each sample (**Figure 4**), the salinity span was found to be relatively wide in the northern slope of the Tazhong area. The NaCl mass fraction salinity (w (NaCl)%) was in the range of 0.88–22.38%. In addition, the closer the calcite sample was to unconformity, the more likely that it contained low-salinity inclusions. However, the salinity of the same well, such as LG106, was also significantly different. The salinity of LG106 was in the range of 1.4–7.59% in the gas–liquid phase 1, whereas that of w (NaCl) % was in the range of 21.26–22.38% in gas–liquid phase 2. This also shows that the area was affected by karst fluids with different salinities.

Based on the salinity analysis results, the inclusions can be divided into three types: 1) Low-salinity inclusions, w (NaCl)% 0.88–5%, which were found in LG106, TL201-1H, TL452, and LG171; the sampling point was 0–108 m below the unconformity surface; belonging to the NaCl–KCl–H_2O system; 2) Medium-salinity inclusions, w (NaCl)% 5–15%, which were found in TL201-1H, TL452, LG512, and LG171; the sampling point was 18–108 m below the nonconformity surface; with freezing point temperatures ranging from −12.0 to −5.0°C, belonging to $CaCL_2$–H_2O, NaCl–$CaCl_2$–H_2O, and NaCl–$MgCl_2$–H_2O systems.

According to Boni (1986), the change in the water–salt system is related to the change in the ions in the system, which indicates that Ca (Mg) ions are important components in this type of inclusion fluid. 3) High-salinity inclusions, w (NaCl)% 15–23%. Except for TL452, all the other samples contained high-salinity inclusions. The sampling point was 0–210 m below the unconformity surface, which belongs to $CaCl_2$–H_2O and NaCl–$CaCl_2$–H_2O systems. This also indicates that the Ca ion is an important component in this type of inclusion fluid, and high-salinity inclusions are common in the study area. In addition, there were some extremely low-salinity inclusions, for example, LG106 and LG171, with a minimum w (NaCl)% of 0.88% (**Table 2**), which is much lower than the current seawater salinity of 3.5%.

4.2.2 Homogenization Temperature Characteristics of Gas–liquid Phase Inclusions

The temperature of 273 gas–liquid inclusions was tested in the range of 49–128°C, and the temperatures of Ordovician inclusions in different drilling wells were different (see **Table 2**). There were also differences between different gas–liquid phase inclusions in the same well. For example, the homogenization temperatures of the LG106 gas–liquid phase 1 and gas–liquid phase 2 inclusions were in the ranges of 66–90°C and 78–105°C, respectively (**Table 2**). Overall, the highest temperature in the measured samples was 128°C (**Table 2**, **Figure 5**), the number of such inclusions was small, and there were no extremely high-temperature inclusions (>140°C). This may be related to the small number of samples and the sampling location. According to previous studies, the maximum homogenization temperature of the two-phase gas–liquid brine

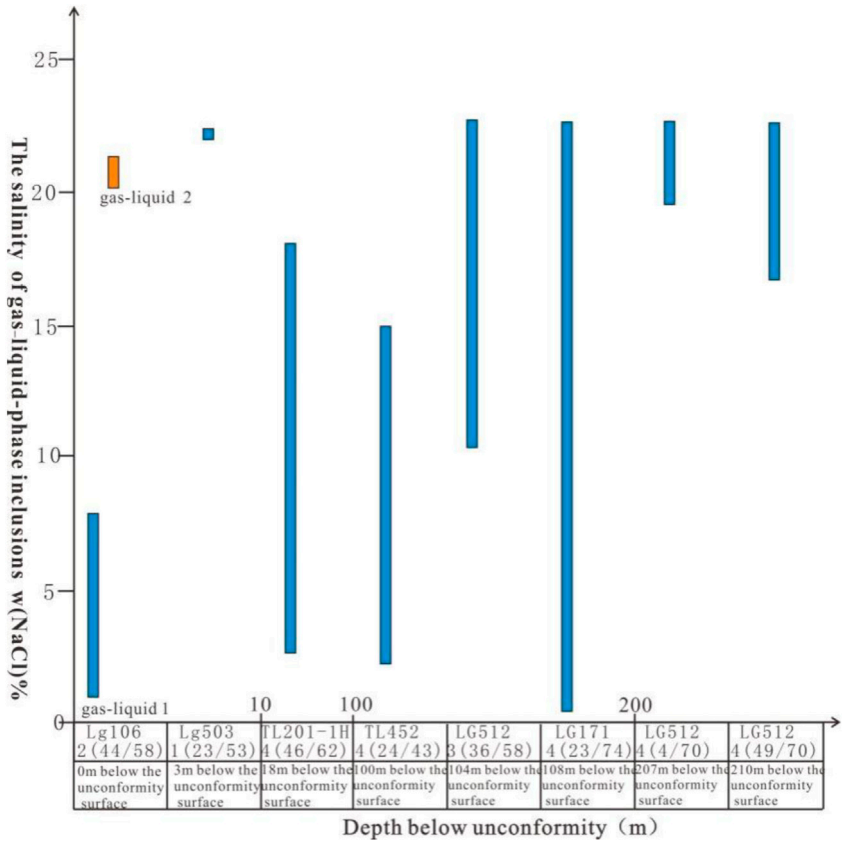

FIGURE 4 | Salinity distribution of gas–liquid inclusions in the northern slope of the Tazhong area.

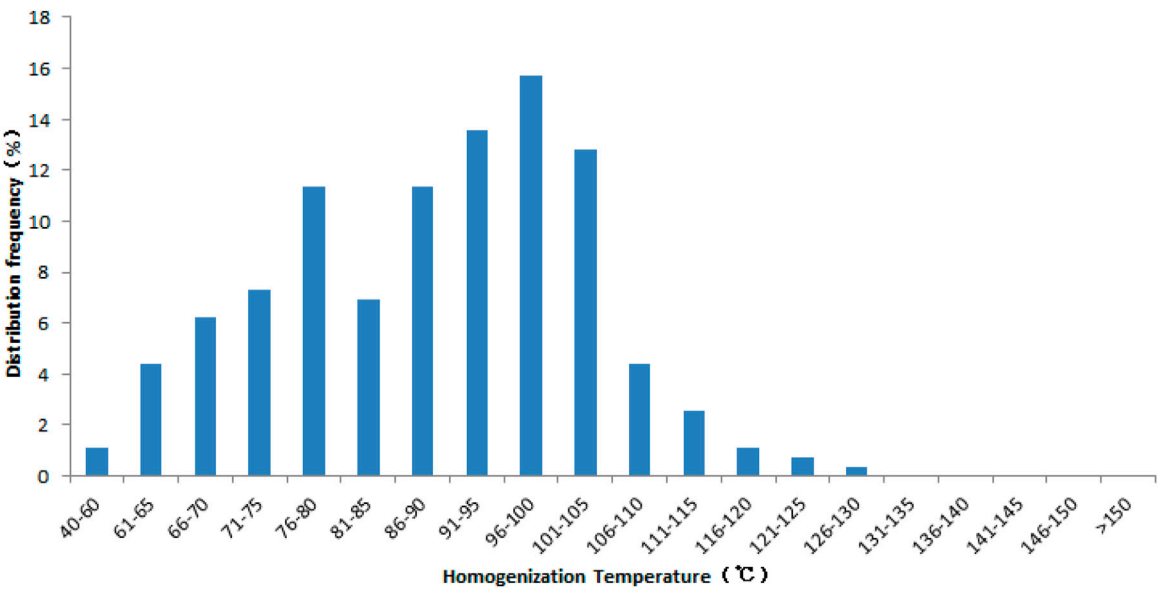

FIGURE 5 | Homogenization temperature distribution of inclusions in calcite from the northern slope of the Tazhong area.

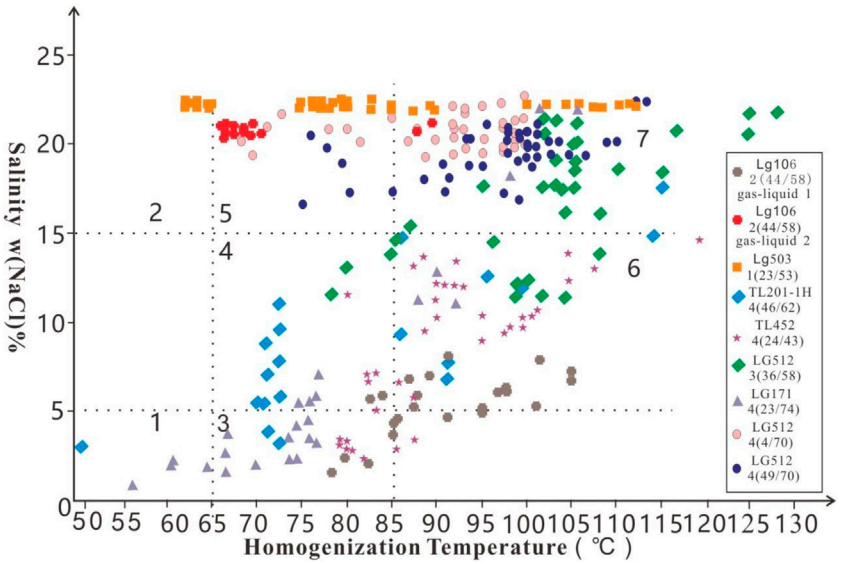

FIGURE 6 | Salinity–homogenization temperature intersection diagram of the two-phase gas–liquid brine inclusions in the northern slope of the Tazhong area, 1-low temperature and low-salinity inclusions; 2-low-temperature and high-salinity inclusions; 3-medium-temperature and low-salinity inclusions; 4-medium-temperature and medium-salinity inclusions; 5-medium-temperature and high-salinity inclusions; 6-high temperature and medium–salinity inclusions; and 7-high-temperature and high-salinity inclusions.

inclusions in the northern slope of the Tazhong area can reach 200°C (Quan, 2020). This shows that there may be an abnormal high-temperature fluid in this area; however, the scope of action is limited. No corresponding samples were obtained this time. On the other hand, low-temperature inclusions were visible (<65°C), and some inclusions had a temperature of only 49°C, for example, in samples close to the unconformity surface such as wells tl201-1h, lg171, and lg503.

Based on the statistical distribution proportion, the main homogenization temperatures of the inclusion formation were found to be in the ranges of 65–85°C and 85–110°C (**Figure 5**). 1) 65–85°C section: The main peak temperature of the inclusion formation was in the range of 75–80°C, which was the main period for the formation of inclusions and karst fillings. 2) 85–110°C section: The main peak temperature of the inclusion formation was in the range of 95–100°C, which was the main period for the formation of inclusions and karst fillings.

4.2.3 Corresponding Characteristics of Homogenization Temperature and Salinity

Based on the salinity–homogenization temperature diagram (intersecting part) (**Figure 6**), 273 samples of eight samples were found to have generally increased temperature, increased salinity, low temperature, and low salinity; these can be divided into seven types of fluid genetic inclusions with different properties: 1) Low-temperature and low-salinity inclusions, 2) Low-temperature and high-salinity inclusions: the homogenization temperature of the two types of inclusions was less than 65°C, the salinity of the low-salinity inclusions was in the range of 0.88–5%, and the salinity of the high-salinity inclusions was in the range of 15–23%; 3) Medium-temperature and low-salinity inclusions, 4) Medium-temperature and medium-salinity inclusions, 5) Medium-temperature and high-salinity inclusions: the homogenization temperature of the above mentioned three types of genetic inclusions was in the range of 65–85°C; however, the salinity value gradually changed from 0.88–5% to 15–23%; 6) High-temperature and medium-salinity inclusions, and 7) High-temperature and high-salinity inclusions. The formation temperature of the above mentioned two types of inclusions was in the range of 85–110°C or even higher, and the salinity was in the range of 5–22%.

Through the analysis of the homogenization temperature and salinity of a single well (**Figure 7**), it is found that the closer to the unconformity surface, the greater the development of the low-temperature and low-salinity inclusions will be; in comparison, the farther away from the unconformity surface, the greater the development of the high-temperature and high-salinity inclusions will be. In addition, the single-well analysis shows that multistage fluid inclusions are recorded in the calcite contained in the sample, and there are more stages near the unconformity. The LG106 2 (44/58) sample was taken from the fracture-cavity calcite near the weathering surface (**Figure 7C**). Gas–liquid phase 1 had a low-medium salinity (some parts had lower and some parts had higher salinity than seawater), with the peak homogenization temperature in the range of 60–70°C. Therefore, the inclusions were of medium temperature and low salinity (**Figure 7C**), with the lowest salinity <3.5%. Similar medium-temperature and low-salinity inclusions also existed in the sample taken from TL452 3 (22/43) (**Figure 7B**). However, the inclusions in the sample taken

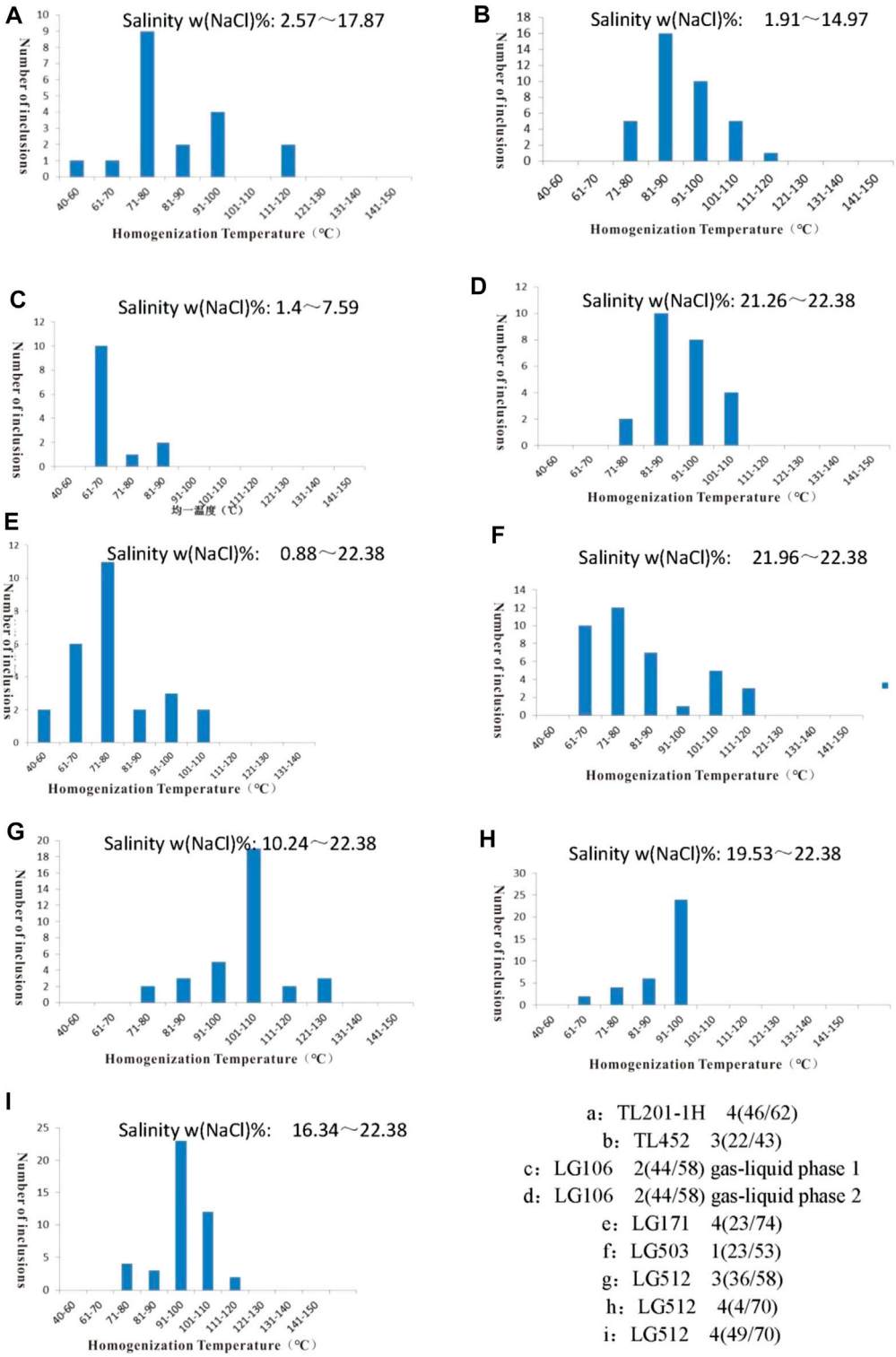

FIGURE 7 | Corresponding relationship between the homogenization temperature and salinity of the inclusions in the northern slope of the Tazhong area. **(A)** Samples taken from TL201-1H 4 (46/62); **(B)** TL452 3 (22/43); **(C)** LG106 2 (44/58), gas–liquid phase 1; **(D)** LG106 2 (44/58), gas–liquid phase 2; **(E)** LG171 4 (23/74); **(F)** LG503 1 (23/53); **(G)** LG512 3 (36/58); **(H)** LG512 4 (4/70); and **(I)** LG512 4 (49/70).

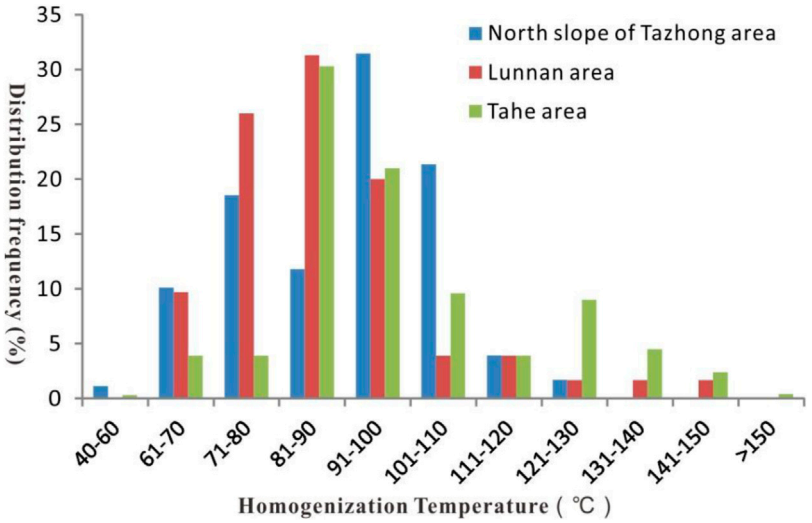

FIGURE 8 | Homogenization temperature distribution of inclusions in Tahe and Lunnan areas, northern Tarim Basin (Dan et al., 2015).

from LG106 2 (44/58) were of high salinity, filled in gas–liquid phase 2, and formed by another period of fluid activity (**Figure 7D**). **Figure 6A** shows the result of the sample taken from TL201-1H 4 (46/62). It was taken from the calcite associated with mud in a cave 18 m below the weathering crust surface. The salinity and homogenization temperature were widely distributed, with the lowest temperatures <65°C. Therefore, the conditions made it possible for the low-temperature and low-salinity and low-temperature and medium-salinity inclusions. In addition, medium-temperature (70–80°C) and high-temperature (110–120°C) inclusions can be seen. The sample LG171 4 (23/74) was taken from the calcite in the dissolved fracture, which was 108 m below the unconformity surface, with a salinity range of 0.88–22.38% and a temperature range of 40–110°C. All types of inclusions existed in this sample, showing the characteristics of continuous fluid activity in multiple periods (**Figure 7E**). Three LG512 samples were taken from the calcite in the dissolution fractures 104, 207, and 210 m below the unconformity surface. The inclusions were mainly of high-temperature and medium–high salinity, with no occurrence of low-temperature and low-salinity inclusions (**Figures 7G–I**).

5 DISCUSSION

5.1 Fluid Activities on Calcite Formation in the Tazhong Area

Dan et al. (2015) found that the peak homogenization temperatures of inclusions in Tahe and Lunnan Oilfields in the Tarim Basin were in the ranges of 85–95°C and 80–90°C, respectively. The inclusions were formed in the similar temperature range in Tahe and Lunnan areas (**Figure 8**). Evidently, the peak homogenization temperature (90–100°C) of most inclusions in the Tazhong area was higher than that in the previously mentioned two areas. This indicates that the tectonic settings of Tahe and Lunnan were similar and that the diagenetic fluid activity was the same during the burial diagenetic period, while it was different in the Tazhong area. In addition, high-temperature (>140°C) inclusions were found in the Tahe and Lunnan Oilfields, indicating the influence of hydrothermal activity. However, no such high-temperature inclusions were found in the samples taken from the Tazhong area. The formation of karst fractures and caves in the Yingshan Formation in this area might be less affected by abnormally high-temperature hydrothermal fluid activities, but predominantly by the fluid activities during the normal burial period. Moreover, there were low-temperature (<65°C) inclusions in the three areas, indicating that they were all influenced by the low-temperature fluid activities during the exposure period.

5.2 Karst and Filling Stages and Fluid Properties in the Tazhong Area

Based on the tectonic background and division of fracture stages in the core, the Tazhong area is found to have experienced multistage tectonic movement, resulting in fluid activity, fracture, karst, and filling of carbonate rocks. In the Middle–Late Ordovician exposure period, the mud in the fracture cave was filled with calcite, and in the Middle–Late Ordovician and Silurian Devonian, the filling was fracture calcite. The inclusion test showed two stages of fluid activity after the formation of the fracture cave and fracture. The homogenization temperatures of the inclusions were analyzed from the burial history map of the area. The two homogenization temperature ranges of the inclusions were just in the two burial periods of Middle Hercynian and Late Hercynian (**Figure 9**). In the Caledonian period, the dissolution fracture cave formed by karst and the fracture formed by Silurian Devonian tectonic activity were exposed, and two large-scale fillings occurred in the Middle Hercynian and Late Hercynian periods.

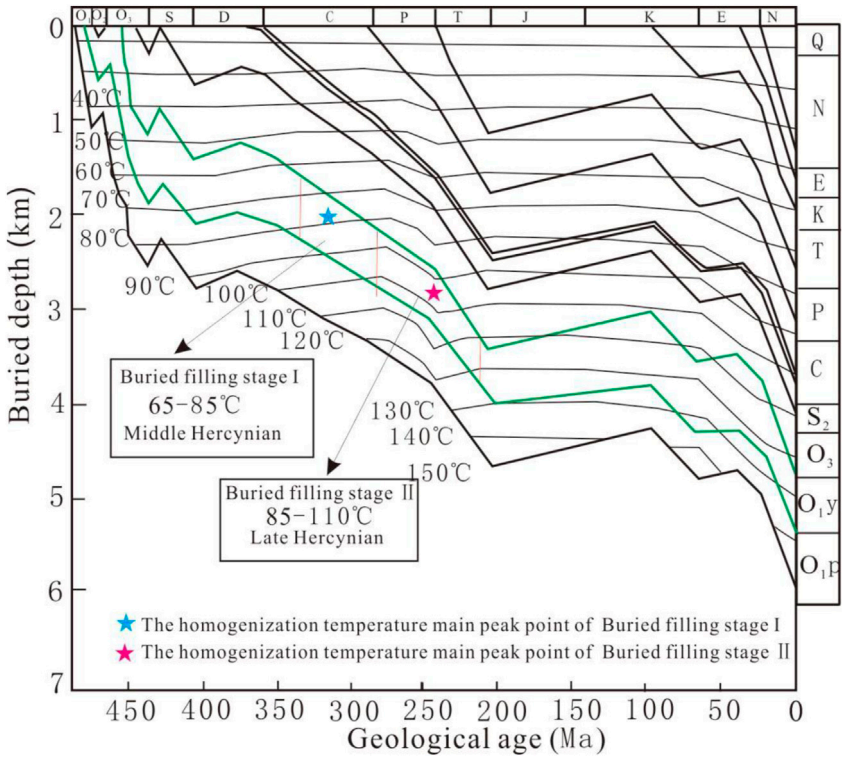

FIGURE 9 | Burial history map of the Ordovician Karst stage from Well TL162 in the Tazhong area (Base Map Burial History Map by (Zhao et al., 2007).

In addition, many evidences point to low-temperature low-salinity karsts in the Yingshan Formation exposure period in this area, and many types of fluids were identified:

1) A large number of irregularly distributed liquid-phase inclusions were formed in the calcite crystals (**Table 1**). The liquid-phase inclusions might have been formed by the leakage of multiphase inclusions due to the late tectonic action or by the formation of inclusions in an environment where the temperature is lower than 50°C (Wu et al., 2010). This low-temperature environment did not produce gas-phase inclusions. Therefore, it can be inferred that part of the liquid-phase inclusions was formed in the normal-temperature environment, that is, these inclusions were formed on the surface or near the surface in the Middle Caledonian period.
2) The homogenization temperature of the inclusions was lower than 65°C, and the lowest temperature was 49°C. Wu et al. (2010) also considered that 50–65°C can be classified as the temperature range near the surface subsurface flow zone. Based on the analysis of the burial history map, these inclusions were also exposed to the surface or near the surface in the Middle Caledonian (**Figure 9**). The salinity analysis showed that the low-temperature inclusions were of low or high salinity, reflecting the existence of freshwater or seawater karst environment, while the surface was exposed in the Middle Caledonian period.
3) Some medium-temperature inclusions (65–85°C) had extremely low salinity (**Figures 7B,C**), which was lower than that of seawater. Liu et al. (2008) found that the existence of freshwater salinity indicated the formation of calcite in the low-temperature environment of surface karst. Moreover, the freshwater salinity indicated that the inclusions were affected by the rebalancing effect, which caused an increase in the homogenization temperature. However, the fluid in some inclusions did not exchange heat with the outside environment, and the salinity of the fluid remained the same.

Through the above mentioned analysis, it can be found that there were three main stages of karst or filling development in the Yingshan Formation in the Tazhong area: Middle Caledonian exposed karst, Middle Hercynian buried filling, and Late Hercynian buried filling. The calcite formed by Middle Caledonian exposed karst mainly comprised three types of liquid-phase inclusions: low-temperature low salinity, medium-temperature low salinity, and low-temperature high-salinity inclusions. The calcite inclusions formed in the Middle Hercynian buried filling were dominated by medium-temperature medium-salinity inclusions and medium-temperature high-salinity inclusions. The calcite inclusions formed in the Late Hercynian buried karst were dominated by high-temperature medium-salinity inclusions and high-temperature high-salinity inclusions.

TABLE 3 | Types of inclusions and paleokarst environment in the northern slope of Tazhong area.

Inclusion type		Homogenization T (°C)	Karst system	Paleo environment	Formation period
Liquid Phase	Normal	Freshwater/seawater	Exposed freshwater/seawater karst	Middle Caledonian	
Gas–liquid phase	LTLS[a]	<65	Salinity 0.88–5%	Exposed freshwater karst	
	MTLS[a]	65–85	NaCl-KCl-H_2O system		
	LTMS[a]	<65	Salinity 5–15%, NaCl-$CaCl_2$-H_2O or NaCl-$MgCl_2$-H_2O system	Exposed seawater karst	
	MTMS[a]	65–85	Salinity 5–15%, NaCl-$CaCl_2$-H_2O or NaCl-$MgCl_2$-H_2O system	Buried filling stage I	Middle Hercynian
	MTHS[a]		Salinity 15–22.38%, $CaCl_2$-H_2O or NaCl-$CaCl_2$-H_2O system		
	HTMS[a]	85–110	Salinity 5–15%, $CaCl_2$-H_2O-$MgCl_2$ or NaCl-$MgCl_2$-H_2O system	Buried filling stage II	Late Hercynian
	HTHS[a]		Salinity 15–22.38%, $CaCl_2$-H_2O-$MgCl_2$ or NaCl-$MgCl_2$-H_2O system		

[a]*LTLS: low-temperature low-salinity; MTMS: medium-temperature medium-salinity; LTMS: low-temperature medium-salinity; MTMS: medium-temperature medium-salinity; MTHS: medium-temperature high-salinity; HTMS: high-temperature medium-salinity; HTHS: high-temperature high-salinity.*

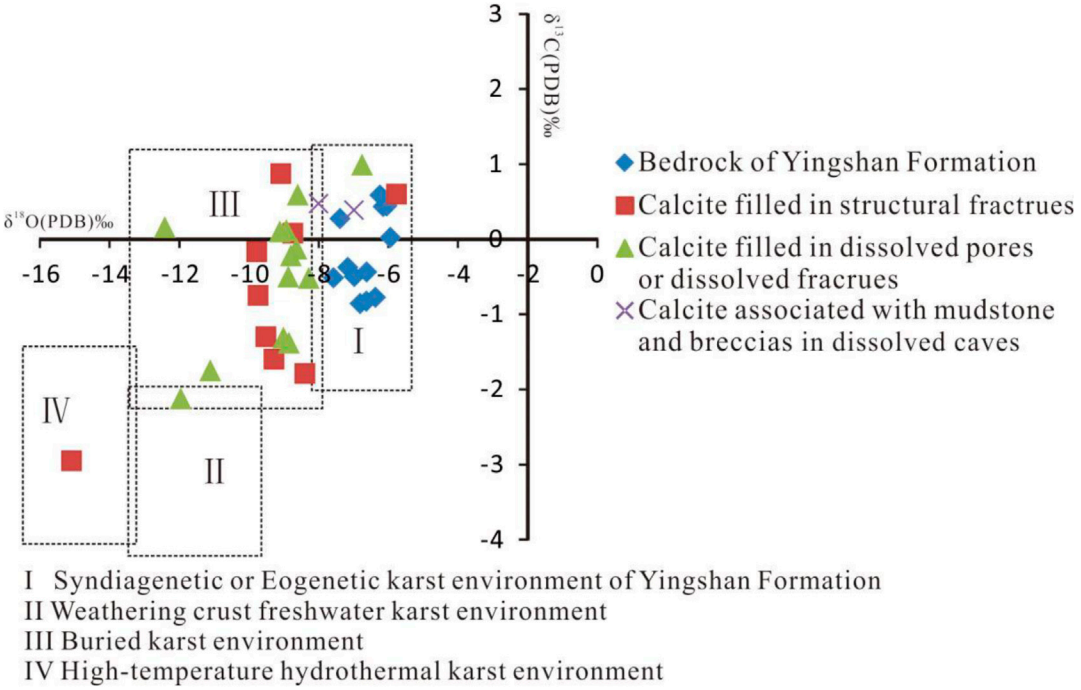

FIGURE 10 | Carbon and oxygen isotopic characteristics of fracture-cave calcite in the northern slope area of Tazhong (Dan et al., 2019).

Table 3 shows the specific stages and fluid parameters of each stage.

Dan et al. (2019) found that calcite was mainly formed in the Middle Caledonian syndiagenetic or eogenetic karst environment and burial environment, and small amounts of calcite were formed in the buried high-temperature environment and Middle Caledonian weathering crust karst environment (**Figure 10**). A large number of structural fractures and solution fracture calcite were formed during burial, and the cave was filled with mud. Calcite was developed in the exposure environment of early diagenetic mixed water, consistent with the inclusion data.

5.3 Indication of Paleokarst Reservoir Development

Most of the fracture-cavity reservoirs in the northern slope of the Tazhong area were filled with mud, which had a significant

influence on reservoir development. Through the testing of calcite inclusions associated with mud in the TL201-1H karst cave, the main karst fluids formed in this area can be accurately determined. Furthermore, when testing the TL201-1H sample, low-temperature low-salinity inclusions and low-temperature medium-salinity inclusions were found (**Figure 6A**), proving the existence of freshwater and seawater fluids in these fractures and caves. These results correspond to the results of cathodoluminescence analysis. Limestone grain edges and cements in the TL201-1h inclusions showed bright luminescence, reflecting the influence of meteoric water. The associated calcite cathodoluminescence was dark, reflecting the influence of seawater (**Figure 2J**). In addition, Dan et al. (2019) found the presence of carbon and oxygen isotopes of calcite associated with mud in another well, showing similar results of bedrock and also reflecting the characteristics of early karst environment (**Figure 10**). The above mentioned results showed that eogenetic karstification may be the key factor in the formation of reservoirs in the Tazhong area.

After the formation of the early diagenetic karst fracture cave reservoir in central Caledonia and the formation of the structural fracture reservoir caused by Silurian Devonian strike slip, the large-scale calcite growth in the middle Hercynian and Late Hercynian burial periods reflected by the inclusions was studied, as discussed in **Section 5.2**. The results point to further filling of the early fracture cave reservoir, reduction in reservoir space, and enhancement in reservoir heterogeneity.

6 CONCLUSION

A test was conducted on calcite inclusions in the fracture cave of the northern slope of the Tazhong area. The results showed that most of the inclusions were single-liquid phase and gas–liquid two-phase inclusions, while some of them contained gas-phase or liquid-phase hydrocarbons. The inclusions assumed various shapes, mainly in free form, small groups, and distributed along microfractures in the crystal. The number of single liquid-phase inclusions was more than that of two-phase gas–liquid inclusions. The two-phase gas–liquid inclusions in the study area could be divided into seven types: low-temperature low-salinity; low-temperature high-salinity; medium-temperature low-salinity; medium-temperature medium-salinity; medium-temperature high-salinity; high-temperature medium-salinity; and high-temperature high-salinity inclusions. They have the characteristics of positive correlation between high temperature and high salinity and low temperature and low salinity. The closer to the unconformity surface, the greater the development of low-temperature and low-salinity inclusions will be; the further away from the unconformity surface, the greater the development of high-temperature and high-salinity inclusions will be. Based on a comprehensive analysis of the burial history, three stages of fluid action were judged in the northern slope of the Tazhong area: Middle Caledonian exposed karst stage, Middle Hercynian buried filling stage I, and Late Hercynian buried filling stage II. By testing the calcite inclusions associated with mud in the karst cave and combining with previous research, it is judged that the Middle Caledonian period is associated with early diagenetic atmospheric fresh water and seawater karstification, which is key to the formation of karst reservoirs in this area. Two instances of burial filling in the Middle and Late Hercynian periods destroyed the reservoir and led to enhanced reservoir heterogeneity.

DATA AVAILABILITY STATEMENT

The original contributions presented in the study are included in the article/Supplementary Material, further inquiries can be directed to the corresponding author.

AUTHOR CONTRIBUTIONS

Conceptualization: YD and GN; methodology: YD; formal analysis: YD; investigation: BL, QZ and GN; writing—original draft preparation: YD; writing—review and editing: JB and YD; project administration: BL; All the co-authors performed a critical revision of the intellectual content of the study.

FUNDING

This research was funded by the Natural Science Foundation of Guangxi, China (2020GXNSFAA297095, 2021AB29005, 2020AB22013), the National Key R&D Program of China (No. 2018YFC0604301, 41902261), the Nonprofit Industry Research Program of the Chinese Academy of Geological Sciences (YYWF201723), the Geological Survey Program of the China Geological Survey (DD20190723, DD20221658), the basic research program of Institute of Karst Geology, Chinese Academy of Geological Sciences (2020012, 2020018).

ACKNOWLEDGMENTS

Prof. Pan Wen-Qing and Senior Engineer Zhang Zheng-Hong of the Research Institute of Exploration and Development at Tarim Oilfield Company of Petro China have been of great assistance during the core observations and sample collection processes.

REFERENCES

Bodnar, R. J. (1992). *Revised Equation and Table for Freezing point Depressions of H2O-Salt Fluid Inclusions*. Program and Abstracts. Lake Arrowhead, CA: Geoarabia Journal of the Middle East Petroleum Geosciences. 14, 15.

Boni, M. (1986). The Permo-Triassic Vein and Paleokarst Ores in Southwest Sardinia: Contribution of Fluid Inclusion Studies to Their Genesis and Paleoenvironment. *Mineralium Deposita* 21 (1), 53–62. doi:10.1007/BF00204362

Cai, C. F., Li, K. K., Cal, L. L., Li, B., and Jiang, L. (2009). Geochemical Characteristics and Origins of Fracture-And Vug-Fillings of the Ordovician in Tahe Oilfield, Tarim Basin. *Acta Petrologica Sinica* 25 (10), 2399–2404.

Chen, H. H., Li, C. Q., and Zhang, X. M. (2003). The Use of Fluid Inclusions to Determine Tahe Oil and Gas Accumulation Periods and the Main Accumulation Period. *Earth Sci. Front.* 10 (1), 265–270.

Chen, H. H., Wu, Y., and Zhu, H. T. (2016). Eogenetic Karstification and Reservoir Formation Model of the Middle-Lower Ordovician in the Northeast Slope of Tazhong Uplift (In Chinese with English Abstract), Tarim Basin. *Acta Petrolei Sinica*, 1231–1246. doi:10.7623/syxb201610003

Chen, X. S., Yi, W. X., and Lu, W. Z. (2004). The Paleokarst Reservoirs of Oil/Gas Fields in China. *Acta Sedimentologica Sinica* 22 (2), 243–252.

Dan, Y., Liang, B., and Cao, J. W. (2012). Geochemical Features and Environmental Significances of Deposits in Ordovician Karstic Fractures and Caves, Lunnan Area, Tarim Basin. *Pet. Geology. Exp.* 34 (6), 623–628. doi:10.11781/sysydz201206624

Dan, Y., Liang, B., Cao, J. W., Zhang, Q. Y., and Hao, Y. Z. (2015). Eogenetic Karstification in Carbonatite and its Significance for Hydrocarbon Geology. *Carsologica Sinica* 34, 126. doi:10.11932/karst20150205

Dan, Y., Lin, L., Liang, B., Zhang, Q., Cao, J., and Li, J. (2019). Geochemistry of the Fracture-Cave Calcite of the Ordovician Yingshan Formation and its Paleokarst Environment in the Tazhong Area, Tarim Basin, China. *Carbonates Evaporites* 34, 1511–1524. doi:10.1007/s13146-019-00500-8

Dan, Y., Lin, L., Liang, B., Zhang, Q., Yu, Y., Cao, J., et al. (2018). Eogenetic Karst Control of Carbonate Reservoirs During a Transient Exposure: a Case Study of the Ordovician Yingshan Formation in the Northern Slope of the Tazhong Uplift, Tarim Basin, China. *Minerals* 8 (8), 345. doi:10.3390/min8080345

Dan, Y., Nie, G., Liang, B., Zhang, Q., Li, J., Dong, H., et al. (2021). The Source of Fracture-Cave Mud Fillings of the Ordovician Yingshan Formation and its Paleokarst Environment in the Northern Slope of the Tazhong Uplift, Tarim Basin, China: Based on Petrology and Geochemical Analysis. *Minerals* 11 (12), 1329. doi:10.3390/min11121329

Feng, R., Ouyang, C., Pang, Y., Li, Z., Luo, X., Zhang, Q., et al. (2014). Evolution Modes of Interbedded Weathering Crust Karst: A Case Study of the 1 St and 2 Nd Members of Ordovician Yingshan Formation in EPCC Block, Tazhong, Tarim Basin. *Pet. Exploration Dev.* 41, 49–59. doi:10.1016/s1876-3804(14)60005-7

He, J., Han, J. F., and Pan, W. Q. (2007). Hydrocarbon Accumulation Mechanism in the Giant Buried Hill of Ordovician in Lunnan Paleohigh of Tarim Basin. *Acta Petroleo Sinica* 28 (2), 44–48. doi:10.1016/S1872-5813(07)60034-6

Lan, X., Lü, X., Zhu, Y., Yu, H., Zhou, J., and Zhu, F. (2014). Characteristics and Differential Accumulation of Oil/Gas in Lower Paleozoic Marine Carbonate on Northern Slope of Tazhong Low Rise, Tarim Basin, NW China: a Case Study of Lower Ordovician Yingshan Formation. *Arab J. Geosci.* 7, 4487–4498. doi:10.1007/s12517-013-1091-2

Liu, C. G., Zhang, Y., and Lu, H. T. (2008). Genesis and Evolution of Gigantic Calcites in Paleokarstic Caves of Middle-Lower Ordovician in Tahe Oilfield. *Geol. Sci. Tech. Inf.* 27 (4), 33–38.

Liu, D. H., Lu, H. Z., and Xiao, X. M. (2007). *The Application of Fluid Inclusions in Oil and Gas Exploration Research [M]*. Guangzhou: Guangdong Science and Technology Press, 9–19.

Liu, X. (1991). Carbonate Rock and mineral Inclusions in Logistics the Main Body of Research Method and its Application. *Exp. Pet. Geology* 13 (4), 399–401. doi:10.11781/sysydz199104399

Lu, H. Z. (1990). *Fluid Inclusion Geochemistry*. Beijing: Geological Publishing House, 6–53.

Ni, X. F., Shen, A., and Pan, W. Q. (2013). Geological Modeling of Excellent Fractured-Vuggy Carbonate Reservoirs: A Case Study of the Ordovician in the Northern Slope of Tazhong Palaeouplift and the Southern Area of Tabei Slope, Tarim Basin. *Pet. Exploration Dev.* 40, 414–422. doi:10.1016/s1876-3804(13)60056-7

Pang, H., Chen, J., Pang, X., Liu, L., Liu, K., and Xiang, C. (2013). Key Factors Controlling Hydrocarbon Accumulations in Ordovician Carbonate Reservoirs in the Tazhong Area, Tarim Basin, Western China. *Mar. Pet. Geology* 43, 88–101. doi:10.1016/j.marpetgeo.2013.03.002

Quan, H. (2020). *Fluid Environment and Geological Model of Ordovician Reservoir in Northern Slope of Central Tarim Basin*. Beijing: China University of Petroleum.

Shu, Z. G., Zhu, Z. D., and He, X. P. (2008). Reservoir Characteristics of Palaeokarsts in the Tazhong Uplift. *Xinjiang Geology* 26 (3), 274–278. doi:10.3969/j.issn.1000-8845.2008.03.012

Wu, M., Zeng, C. B., and Huang, S. J. (2010). Fluid Inclusion Study of the Ordovician Carbonate Rock Reservoir in the Tahe Oilfield. *Geology China* 37 (5), 1360–1373. doi:10.3724/SP.J.1011.2010.01081

Xia, R. Y., Tang, J. S., and Zou, S. Z. (2006). The Northern Margin of the Tarim Basin Paleokarst Filling Characteristics of Fluid Inclusions. *Carsologica Sinica* 25 (3), 246–249.

Xia, R. Y., and Tang, J. S. (2004). Indication of Mineral Inclusion Characteristics to Palaeokarst Actions. *Acta Geosci. Sinica* 25 (3), 373–377. doi:10.1007/BF02911033

Xu, K., Liu, S., and Yu, B. S. (2012). Fracture Development Characteristics and Logging Responses of Ordovician Carbonate Reservoirs in the Tazhong Area of the Tarim Basin. *Chin. Foreign Energ.* 17 (9), 45–50.

Yan, X. B., Han, Z. H., and Li, Y. H. (2002). Reservoir Characteristics and Formation Mechanisms of the Ordovician Carbonate Pools in the Tahe Oilfield. *Geol. Rev.* 48, 619–626. doi:10.1080/12265080208422884

Yan, X. B., Li, T. J., and Zhang, T. (2005). Differences Between Formation Conditions of Ordovician Karstic Reservoirs in Tazhong and Tahe Areas. *Oil Gas Geology* 26 (2), 202–209. doi:10.3321/j.issn:0253-9985.2005.02.013

Yang, H. J., Han, J. F., and Sun, C. H. (2011). A Development Model and Petroleum Exploration of Karst Reservoirs of Ordovician Yingshan Formation in the Northern Slope of Tazhong Palaeouplift. *ActaPetrolei Sinica* 32, 199–205. doi:10.1007/s12182-011-0123-3

Yu, H. F., Bai, Z. K., and Deng, L. P. (2011). Determination and Geologic Significance of Yingshan Unconformity of Lower Ordovician in Tazhong Area, Tarim Basin. *Xinjiang Pet. Geology* 32, 231–234. doi:10.1007/s12182-011-0123-3

Zhang, Q. Y., Liang, B., and Qin, F. R. (2016). Environmental and Geochemical Significance of Carbon and Oxygen Isotopes of Ordovician Carbonate Paleokarst in Lunnan, Tarim Basin. *Environ. Earth Sci.* 75, 1074–1079. doi:10.1007/s12665-016-5882-0

Zhao, W. Z., Shen, A. J., Pan, W. Q., Zhang, B. M., Qiao, Z. F., and Zheng, J. F. (2013). A Research on Carbonate Karst Reservoirs Classification and its Implication on Hydrocarbon Exploration: Cases Studies from Tarim Basin. *Acta Petroleo Sinica* 29, 3213–3222. doi:10.1086/671395

Zhao, Z. J., Wang, Z. M., Wu, X. N., and Chen, X. S. (2007). Genetic Types and Distribution Forecast of Available Carbonate Reservoirs in Ordovician in the Central Area of Tarim Basin. *Pet. Geology. Exp.* 29 (1), 40–46. doi:10.1016/S1872-5813(07)60034-6

Zhu, G. Y., Zhang, S. C., Wang, H. H., Yang, H. J., Meng, S. C., and Gu, Q. Y. (2009). The Formation and Distribution of Deep Weathering Crust in North Tarim Basin. *Acta Petrologica Sinica* 25, 2384–2398. doi:10.1016/S1874-8651(10)60080-4

Conflict of Interest: The authors declare that the research was conducted in the absence of any commercial or financial relationships that could be construed as a potential conflict of interest.